Polymer 51 (2010) 4218–4224

Contents lists available at ScienceDirect

Polymer

journal homepage: www.elsevier.com/locate/polymer

A new method for achieving nanoscale reinforcement of biaxially oriented polypropylene film

Yijian Lin, Anne Hiltner*, Eric Baer

Department of Macromolecular Science and Engineering, Case Western Reserve University, Cleveland, OH 44106-7202, USA

ARTICLE INFO

Article history:
Received 9 May 2010
Received in revised form
24 June 2010
Accepted 30 June 2010
Available online 7 July 2010

Keywords:
Biaxially oriented polypropylene
Gas barrier
Nanolayers

ABSTRACT

Nanolayers of poly(ethylene oxide) (PEO) produced by layer-multiplying coextrusion crystallize as single, high aspect ratio lamellae that resemble large single crystals. The confined crystallization habit imparts two orders of magnitude reduction in the gas permeability. We now demonstrate how the highly oriented lamellar nanolayers can be obtained with biaxial stretching. For this purpose, we chose biaxially oriented polypropylene (BOPP) film for modification and incorporated PEO nanolayers under conditions that mimicked the typical fabrication process. Sheet that contained a center core with 33 alternating layers of polypropylene (PP) and PEO was coextruded and subsequently biaxially oriented at 145 °C. Biaxial stretching reduced the PEO layer thickness from the spherulitic microscale to nanolayers of highly oriented PEO single lamellae. The nanolayers improved the oxygen barrier by an order of magnitude without sacrificing the high clarity and good tear resistance of BOPP film.

1. Introduction

The demand for higher performance polymeric materials that can also meet today's environmental and energy requirements, has challenged researchers to innovate new materials systems and processes. Most strategies for enhancing the property window rely on the complex, hierarchical structures that are imparted to polymers by melt or solid state processing. A single polymer, or synergistic combinations of two (or more) polymers may be used to optimize the property spectrum; however, advances to existing materials and processes generally achieve only incremental improvements. Nanoscience promises a technology breakthrough that would define the next generation of advanced polymeric materials, particularly materials with an order of magnitude higher gas barrier [1,2].

Nanoparticles with high aspect ratio are an attractive candidate for this purpose. Following the initial success with nylon 6 [3,4], exfoliated organosilicate platelets received an extraordinary amount of attention as the reinforcement in polymer matrix nanocomposites [5], with literally thousands of papers published on the subject in the last 10 years. The combination of key property requirements (gas barrier, transparency and toughness) makes polymer film an ideal candidate for nanotechnology. Although success could transform the high volume polyolefin field, a practical melt process for achieving good dispersion of exfoliated organosilicate platelets has proven an elusive goal [6]. The need exists for alternative approaches to achieving the property enhancements envisaged for polymer nanocomposites.

Recently, using layer-multiplying coextrusion, we discovered a morphology that emerges as confined polyethylene oxide (PEO) layers are made progressively thinner. When the thickness is confined to 25 nm by polystyrene or by poly(ethylene-*co*-acrylic acid) (EAA), the PEO crystallizes as single, high aspect ratio lamellae that resemble single crystals [7,8]. Unexpectedly, the confined crystallization habit imparts two orders of magnitude reduction in the gas permeability. The PEO nanolayers potentially can provide the barrier enhancement envisaged with exfoliated organosilicate platelets. However, adapting this discovery to commercial film processes presents certain challenges. Processing of polymer film often includes a post-extrusion stretching step that reduces the thickness and imparts orientation. For example, fabrication of biaxially oriented polypropylene (BOPP) films involves a biaxial stretching process that reduces the thickness of the polypropylene sheet by about 25× and transforms the opaque, brittle spherulites into a transparent, tough, fibrillar network [9]. Thus, although PEO nanolayers could be coextruded with the polypropylene sheet, the nanolayers would be destroyed in the subsequent stretching step and the barrier enhancement would be lost.

Rather than using layer-multiplying coextrusion to produce the nanolayers, we took an innovative approach in which the post-extrusion stretching process was used to produce the high barrier nanolayers in BOPP film. We coextruded a polypropylene (PP) sheet

* Corresponding author.
E-mail address: ahiltner@case.edu (A. Hiltner).

0032-3861/$ – see front matter © 2010 Elsevier Ltd. All rights reserved.
doi:10.1016/j.polymer.2010.06.059

containing thick PEO layers. The micron-thick PEO layers crystallized with an essentially isotropic spherulitic morphology that did not enhance the barrier. However, the thickness of the PEO layers was chosen so that when the sheet was biaxially stretched under conditions typically used for BOPP film, the PEO microlayers melted and were reduced in thickness to nanolayers. At this size scale, the PEO layers recrystallized as oriented lamellar single crystals of very high aspect ratio.

2. Experimental

The PP (H105-03NA) and PEO (PolyOx WSR N80, $M_w = 200$ kg/mol) were obtained from the Dow Chemical Company. The PP and PEO were combined as alternating microlayers using layer-multiplying coextrusion. In the same process, thick monolithic PP skins were added to produce a 3-layer structure. The multilayer coextruded sheets were biaxially oriented using a Brükner Karo IV biaxial stretcher at 135, 140, 145 and 150 °C with a strain rate of 400% s^{-1}. The draw ratios were 5 × 5, 6 × 6 and 7 × 7.

The first heating thermogram was recorded by a Perkin–Elmer Series 7 differential scanning calorimeter (DSC) using a heating rate of 10 °C min^{-1} from 60 to 190 °C. The crystallinity of the PEO was calculated from the melting enthalpy using the heat of fusion, ΔH_0, of 197 J g^{-1} for PEO crystals [10].

To view the layer structure, a small specimen was cut from the coextruded sheet or oriented film and microtomed at −85 °C through the thickness direction. The microtomed surface was examined in a Digital Laboratories Nanoscope IIIa atomic force microscope (AFM) operating in the tapping mode.

The oxygen permeability $P(O_2)$ was measured with a MOCON OX-TRAN 2/20 at 23 °C, 1 atm and 0% relative humidity. Two films prepared under the same conditions were tested to obtain the average permeability. The carbon dioxide permeability $P(CO_2)$ was measured with a MOCON PERM-TRAN C4/40 at the same conditions. The CO_2/O_2 selectivity was calculated as the ratio $P(CO_2)/P(O_2)$.

Wide angle X-ray scattering (WAXS) and small angle X-ray scattering (SAXS) measurements were carried out using a rotating anode X-ray generator (Rigaku RU 300, 12 kW) equipped with two laterally graded multilayer optics in a side-by-side arrangement, giving a highly focused parallel beam of monochromatic CuK_α radiation ($\lambda = 0.154$ nm). For the SAXS measurements, the X-ray beam was aligned at an angle of about 3° relative to the film surface to avoid total reflection. The scattering vector q was calibrated using a silver behenate (AgBe) standard, which had the (001) peak position at $q = 1.076$ nm^{-1}. On the basis of the intensity of the direct beam, all WAXS and SAXS images were corrected for background scattering.

The clarity was characterized by a light transmission measurement [11], in which a film was placed between a light source and a detector. The light transmission T was calculated as

$$T = \sum_{\lambda=400}^{700} I_\lambda / \sum_{\lambda=400}^{700} I_{\lambda,0} \quad (1)$$

where I_λ is the light intensity at wavelength λ, $I_{\lambda,0}$ is the reference light intensity without the film, and 400–700 is the wavelength range of the visible light. To remove the surface scattering effect, mineral oil with refractive index of 1.500 was spread on both surfaces of the films. The diameters of the light source beam and the detector were both approximately 3 mm. The distance between film and detector was 6 mm. Five spots on each film were selected to perform this measurement.

In a standard trouser tear test, the tear energy G_t was calculated as

$$G_t = 2F/t \quad (2)$$

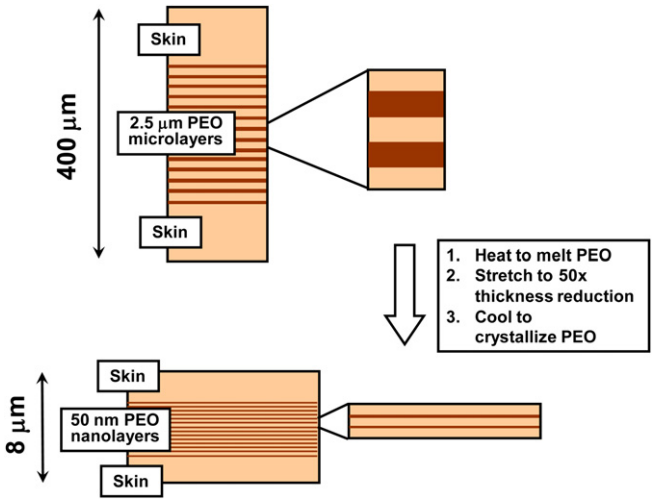

Fig. 1. Schematics showing how polymer microlayers are reduced to nanolayers by biaxial orientation.

where F is the steady force during the tear test and t is the thickness of the film. An Instron 1122 tensile testing machine equipped with a 500 g load cell was employed to record the tear force at a speed of 250 mm min^{-1}.

3. Results and discussion

A 3-layer sheet was produced for biaxial orientation. A 130 μm core layer was prepared by combining PP and PEO as 33 alternating microlayers (17 PP microlayers and 16 PEO microlayers) using layer-multiplying coextrusion [12]. The composition in the core layer was PP/PEO-90/10, 80/20 and 70/30 vol/vol. Two thick 130 μm PP skin layers were added before the melt was spread through a sheet die. The composition of the final 3-layer sheet was PP/PEO 96.7/3.3, 93.3/6.7 and 90/10 vol/vol. The entire architecture was created in a continuous coextrusion process.

The *in situ* transformation of spherulitic PEO layers into impermeable, highly oriented lamellar single crystals is shown in Fig. 1. The typical stretching temperature window for PP film was

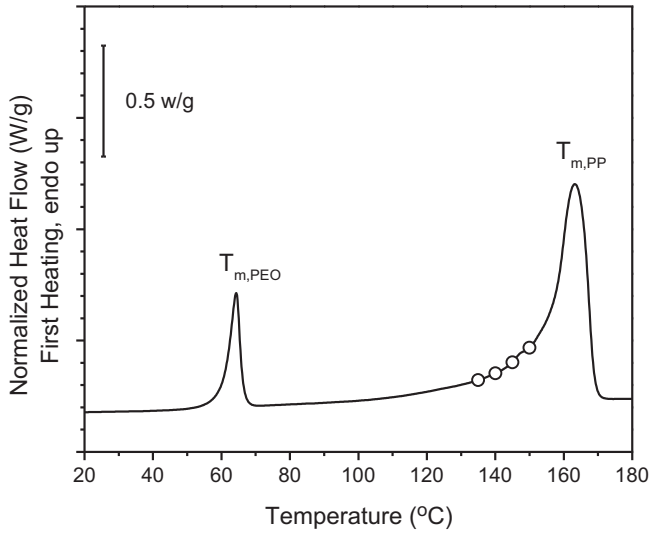

Fig. 2. DSC heating thermogram of extruded PP/PEO sheet with 10 vol.% PEO. The circles indicate the biaxial stretching temperatures that were used to obtain the nano-BOPP films.

135–155 °C [13], close to the PP melting temperature (T_{mPP} of 163 °C), Fig. 2. When the sheet was heated to the stretching temperature, the unoriented PEO spherulites in the thick (0.8-2.4 μm) microlayers melted ($T_{m,PEO}$ of 64 °C). Subsequent biaxial stretching to draw ratios from 5 × 5 to 7 × 7 reduced the thickness of the PEO layers by 25–50×. With the final PEO thickness comparable to the thickness of a single crystal, the PEO recrystallized upon cooling as highly oriented lamellar single crystals of very high aspect ratio. The final biaxially oriented polypropylene film (nano-BOPP) incorporated 16 layers of highly oriented PEO lamellar single crystals.

The AFM images in Fig. 3 compare the 3-layer sheet before and after stretching using the same magnifications. A single PEO microlayer from the core of the coextruded sheet is shown in Fig. 3 (a). The spherulitic morphology of the 2 μm microlayer is clear in the higher resolution images. After stretching to 7 × 7, the nano-BOPP film was reduced in thickness sufficiently that the entire thickness could be imaged readily in the AFM, Fig. 3(b). Higher magnifications show the core layer with 16 PEO nanolayers separated by oriented PP layers, and finally at the highest resolution the individual PEO layers that consisted of very large single lamellae.

A substantial reduction in the oxygen permeability was observed in the nano-BOPP film, by up to a factor of 7 compared to a control film without PEO nanolayers, Table 1. In this set of results, the amount of PEO was constant (10 vol.%) and the biaxial draw ratio was increased from 5 × 5 to 7 × 7. The permeability of the control film decreased somewhat with increasing draw ratio due to tightening of the amorphous tie chains [14]. However, the permeability of the nano-BOPP films decreased proportionally even more.

The permeability of a single PEO layer was extracted by assuming that the film permeability P followed the series model.

$$P_{PEO} = V_{PEO} \Big/ \left(\frac{1}{P} - \frac{V_{BOPP}}{P_{BOPP}}\right)^{-1} \tag{3}$$

where P_{BOPP} and P_{PEO} are the permeabilities of the PP layers and PEO layers, and V_{BOPP} and V_{PEO} are the volume fractions of PP and PEO layers. The value of P_{BOPP} was obtained from a control film that was stretched at the same conditions. Compared to the usual permeability of PEO (0.38 barrer), permeability of the PEO layers in nano-BOPP was reduced by orders of magnitude. Thinner PEO layers, obtained by increasing the draw ratio, resulted in more highly oriented lamellae and lower permeability, Fig. 4. The dependence on layer thickness followed that reported previously for PEO layers produced by coextrusion [7,8]. Thus, the orientation of large single lamellae perpendicular to the flux direction, rather than any specific interactions with the confining PP layers after stretching, was responsible for the exceptional barrier of the PEO nanolayers in nano-BOPP films. The PEO layers were also responsible for a substantial increase in selectivity for CO_2 over O_2. The higher permeability of films with the thinnest PEO layers was attributed to some layer breakup when the layer thickness was reduced below the PEO lamellar thickness of about 25 nm.

The two-phase model for gas transport in semicrystalline polymers assumes that the crystalline core is impermeable and the lamellar fold surfaces constitute the permeable amorphous regions. For oriented lamellar nanolayers, the diffusion pathway depends on the frequency of defects such as lamellar edges. The aspect ratio of the PEO lamellae α was estimated using the Cussler model [15], which assumes that the PEO lamellae are impermeable and oriented perpendicular to the flow.

$$\frac{P}{P_{BOPP}} = \frac{1-v}{1-v+(\alpha v/2)^2} \tag{4}$$

where v is the volume fraction of impermeable PEO crystals in the film, which can be obtained by conversion of the weight crystallinity from DSC, P is the oxygen permeability of the nano-BOPP film and P_{BOPP} is the oxygen permeability of the BOPP control film. As the layer thickness approached the thickness of a single lamella and the constraint became more severe, the PEO lamellae became larger (higher aspect ratio) and more highly oriented, thereby increasing the tortuosity of the gas pathway. The permeability of the nano-

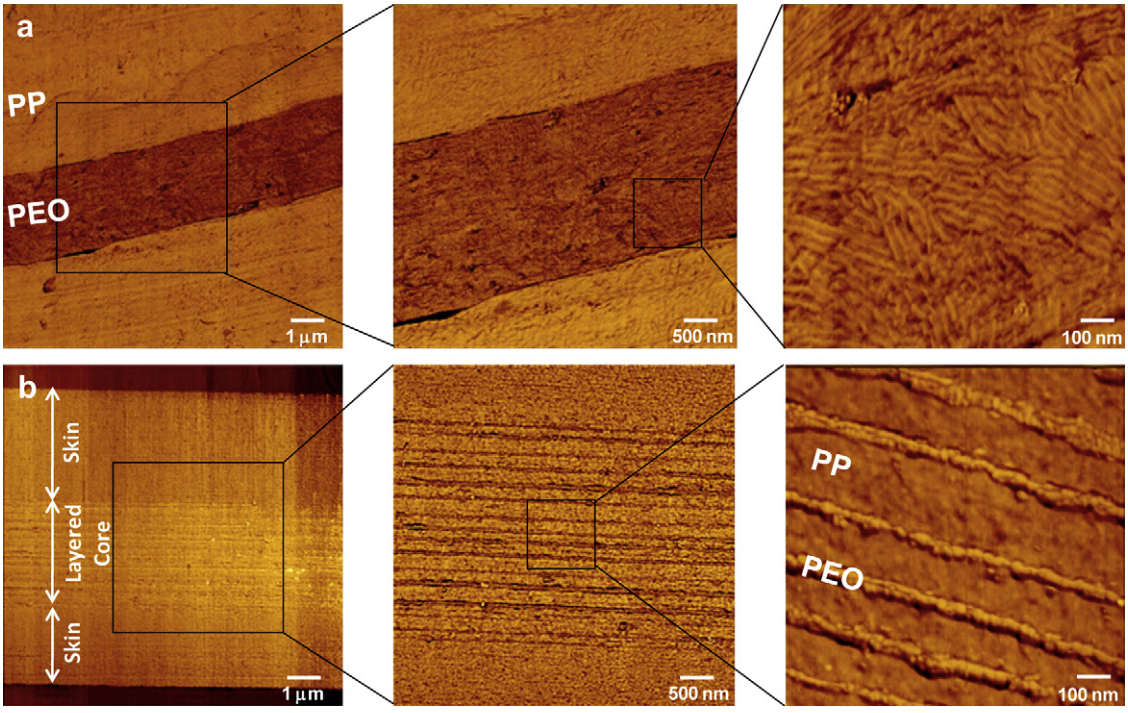

Fig. 3. Cross-section AFM images of PP/PEO-90/10 showing the layer morphology: (a) Before stretching (1 × 1); and (b) after biaxial stretching (7 × 7) at 145 °C.

Table 1
Composition and properties of Nano-Bopp Films.

Sample (PP/PEO-λ) T_d = 145 °C	PEO layer thickness (nm)	Crystallinity of PEO (wt.%)	Fraction of PEO crystals in film, (vol.%) ν	Hermans orientation function of PEO, f_{120}	$P(O_2)$ (barrer)	$P(O_2)_{PEO}$ (barrer)	Aspect ratio of PEO lamellae, α	$P(O_2)$, recrystallized (barrer)	$P(O_2)_{PEO}$, recrystallized (barrer)	Aspect ratio of PEO lamellae, α, recrystallized	Selectivity $P(CO_2)/P(O_2)$, recrystallized
100/0 - 5×5	-	-		-	0.703±0.041			0.685±0.032			3.3
90/10 - 5×5	82	69	6.7	-0.45	0.231±0.001	0.0327	41	0.129±0.004	0.0155	60	10.3
100/0 - 6×6	-	-		-	0.565±0.011			0.538±0.010			3.4
90/10 - 6×6	54	71	6.9	-0.47	0.112±0.002	0.0136	56	0.054±0.001	0.0059	84	11.4
100/0 - 7×7	-	-		-	0.528±0.020			0.488±0.012			3.4
90/10 - 7×7	38	72	7.0	-0.47	0.068±0.007	0.0077	71	0.029±0.004	0.0031	109	10.1

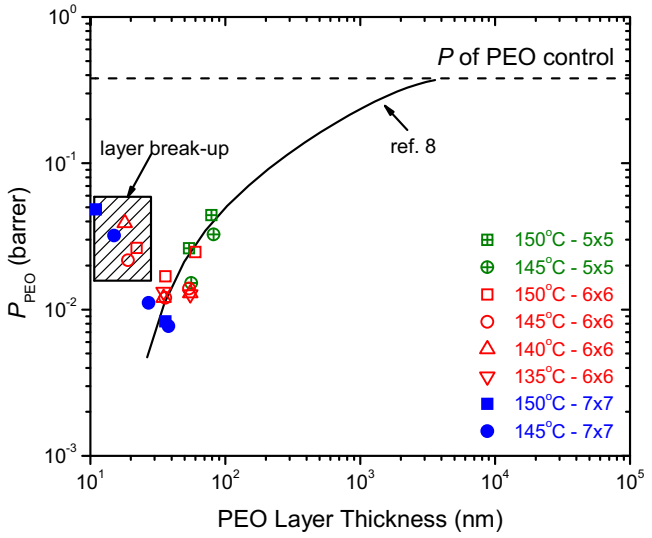

Fig. 4. Effect of layer thickness on the oxygen permeability of the PEO layers. The solid curve is from reference 8.

BOPP film decreased further if the PEO was slowly recrystallized. This was achieved by hydrating the PEO nanolayers at 100% relative humidity and allowing them to slowly recrystallize as more highly ordered lamellae with higher aspect ratio, Table 1.

The wide angle X-ray scattering (WAXS) patterns obtained with the incident beam parallel to the plane of the film (PD) confirmed crystallization of PEO as highly oriented lamellae. The control film stretched at 145 °C to 7 × 7 showed four reflection rings ($2\theta = 14.1°$, 16.9°, 18.6°, 21.8°) from the (110), (040), (130), and (111)/(041) planes of the α-form PP crystals. The concentration of intensity at specific angles revealed the high orientation of PP in the biaxially stretched film, Fig. 5(a,b,c). The PEO layers in nano-BOPP film stretched at 145 °C to 7 × 7 imposed additional features, Fig. 5(d,e). The sharp reflections at $2\theta = 19.2°$ and $2\theta = 23.2°$ were characteristic of the monoclinic form of PEO [16], and were reflections from the (120) planes and the (032) planes, respectively. The sharpness of the PEO reflections revealed a high degree of chain orientation with the *c*-axis aligned normal to the film plane.

It was convenient to describe the degree of orientation by the Hermans orientation function using the PEO (120) plane, f_{120}. Because the (130) reflections from PP ($2\theta = 18.6°$) were close to the (120) reflections of PEO ($2\theta = 19.2°$), the azimuthal intensity profile included intensity from the PP Fig. 5(f). The azimuthal scan was deconvoluted into voigt-shaped peak functions to obtain the intensity from the PEO (120) planes only. The mean square orientation angle of the c-axis of PEO lamellae with respect to the film normal direction was calculated using the intensity distribution profile of the PEO (120) plane according to [8].

$$\left\langle \cos^2 \phi_{120} \right\rangle = \frac{\int_0^{\pi} I_{120}(\phi) \cos^2 \phi \sin \phi d\phi}{\int_0^{\pi} I_{120}(\phi) \sin \phi d\phi} \tag{5}$$

where $I_{120}(\phi)$ was the intensity of the PEO (120) reflections at azimuthal angle ϕ. Hermans orientation function based on the PEO (120) plane, f_{120}, was obtained by

$$f_{120} = \frac{3\langle \cos^2 \phi_{120} \rangle - 1}{2} \tag{6}$$

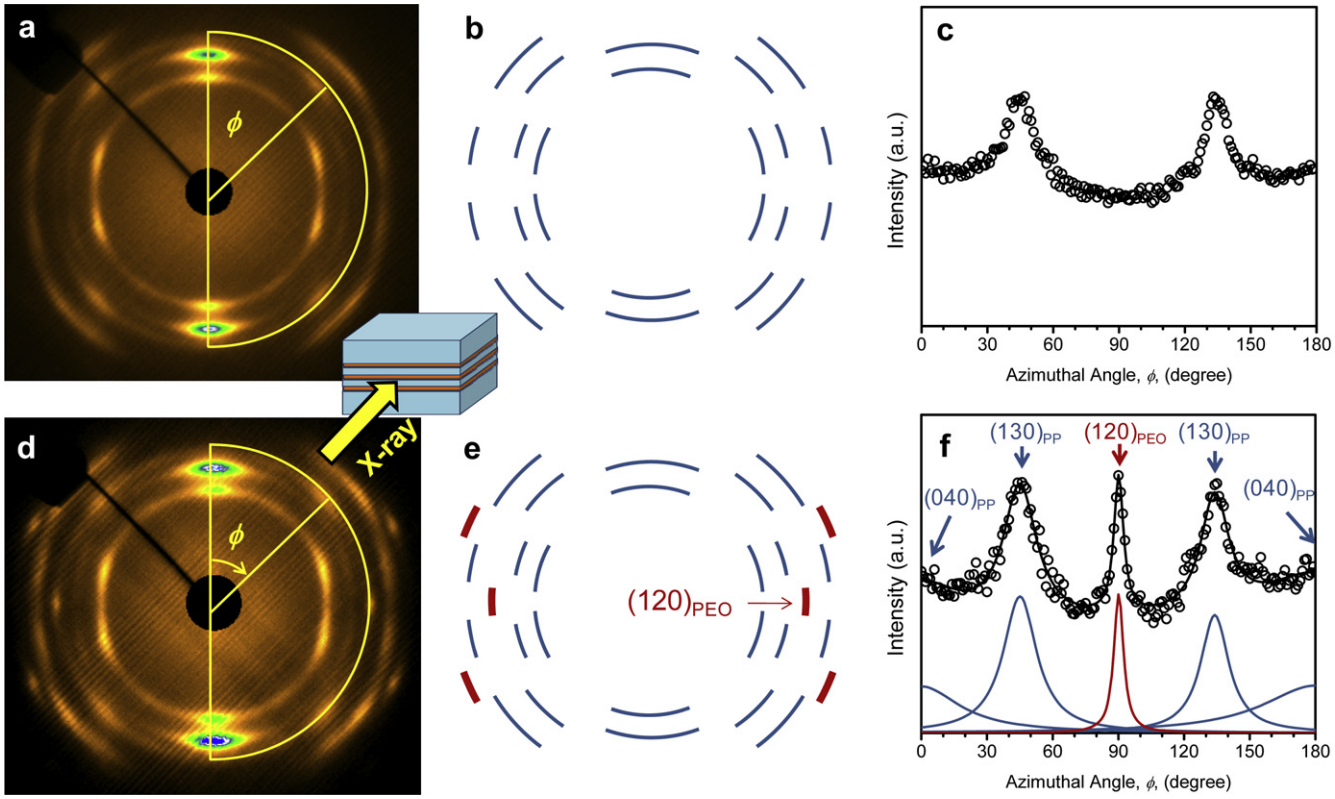

Fig. 5. A comparison of the WAXS pattern of the nano-BOPP film (7 × 7) with that of the control film (7 × 7) reveals additional reflections from the highly oriented PEO lamellae: (a), (b), (c) the WAXD pattern, its schematic representation, and the azimuthal scan at $2\theta = 19.2^{\circ}$ for the control film; and (d), (e), and (f) the same for the nano-BOPP film.

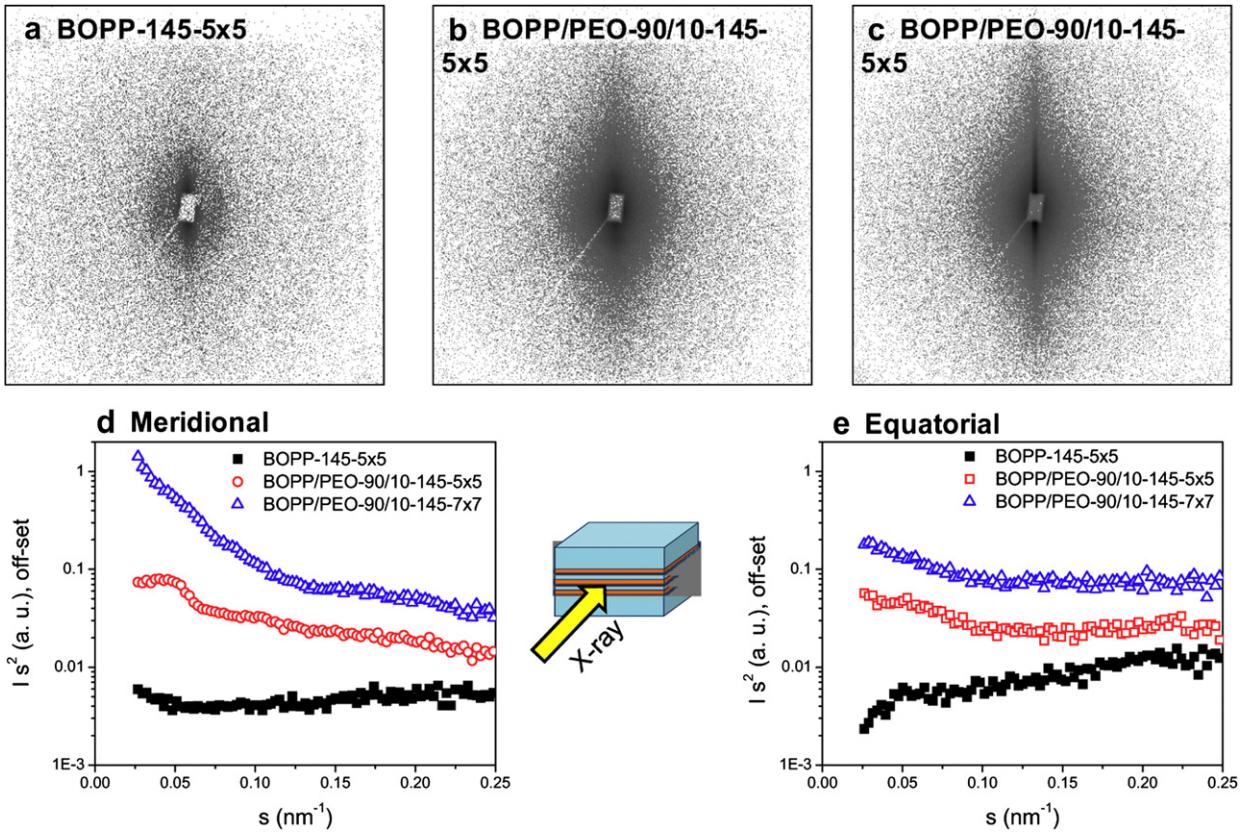

Fig. 6. 2D-SAXS patterns of: (a) BOPP-145-5×5; (b) nano-BOPP/PEO-90/10-145-5×5 with nominal PEO layer thickness of 82 nm; and (c) nano-BOPP/PEO-90/10-145-7×7 with nominal PEO layer thickness of 38 nm. Included are intensity scans along: (d) meridional direction; and (e) equatorial direction.

for perfect in-plane lamellar orientation with *c*-axis normal to the film plane, $f_{120} = -0.5$; for random orientation, $f_{120} = 0$. For nano-BOPP film, $f_{120} = -0.47$ confirmed that the PEO lamellae were well-oriented in the plane of the film with the (120) planes perpendicular to the film plane.

Fig. 6 shows the 2D-SAXS patterns of BOPP control films and two nano-BOPP films with nominal PEO layer thickness of 82 and 38 nm. For all the films, the patterns showed intense meridional streaks that were primarily surface reflections from the film. In order to reveal the contribution from the lamellae, intensity scans were performed in both meridional and equatorial directions. The intensity profiles are included in Fig. 6, where s is the scattering vector and its amplitude is related to the scattering angle 2θ and the X-ray beam wavelength λ as $s = 2(\sin\ \theta)/\lambda$. In the meridional direction, the BOPP control showed a relative flat intensity profile with no discernable peaks. After incorporation of 82 nm PEO layers (nano-BOPP-90/10-145-5×5), a first order correlation peak appeared at $s^* = 0.044$, with corresponding long period $L = 23$ nm ($L = 1/s^*$). This peak was attributed to the in-plane oriented PEO lamellar stacks [8].

When the PEO layer thickness was reduced to 38 nm, close to the lamellar thickness, the first order correlation peak was highly suppressed. This implied that the confinement at this layer thickness prevented formation of lamellar stacks. However, due to the layer thickness distribution, an occasional stack of two or three lamellae could give a peak in the meridional intensity profile. In the equatorial intensity profile, the first order peak was observed at $s^* = 0.052$ for the BOPP control, which corresponded to the long period $L = 19$ nm of PP lamellae that were preferentially oriented perpendicular to the film surface. After incorporation of PEO nanolayers, no additional peaks were seen on the intensity profile, which confirmed that the PEO lamellae were oriented in the plane of the film. This was consistent with the 2D-WAXS results.

The properties of PEO are significantly affected by the relative humidity RH. It was previously found that the permeability of confined PEO layers doubled at 85% RH regardless of the layer thickness [8]. The effect of RH on the permeability of the recrystallized nano-BOPP films was also tested, and the resulting P_{PEO} at 85% RH is compared with P_{PEO} at 0% RH in Fig. 7. Although P_{PEO} at 85% RH was about a factor of 2 higher than P_{PEO} at 0% RH, the dependence on layer thickness was conserved, which indicated that even under high RH only the amorphous regions were affected. Exposure to water did not have an effect on the lamellae, which continued to serve as oriented impermeable platelets to reduce the oxygen permeability.

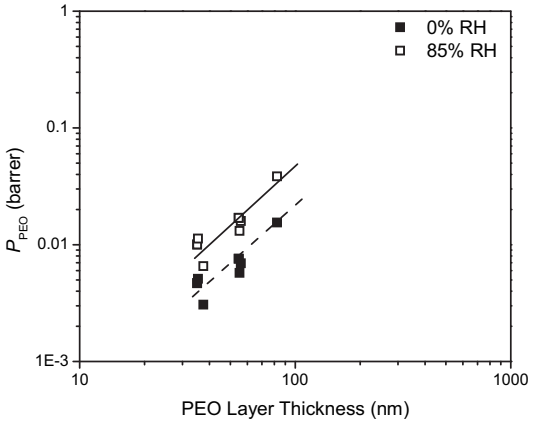

Fig. 7. Effect of moisture on the oxygen permeability of PEO layers. Data shown are from films stretched at 145 and 140 °C without PEO layer breakup.

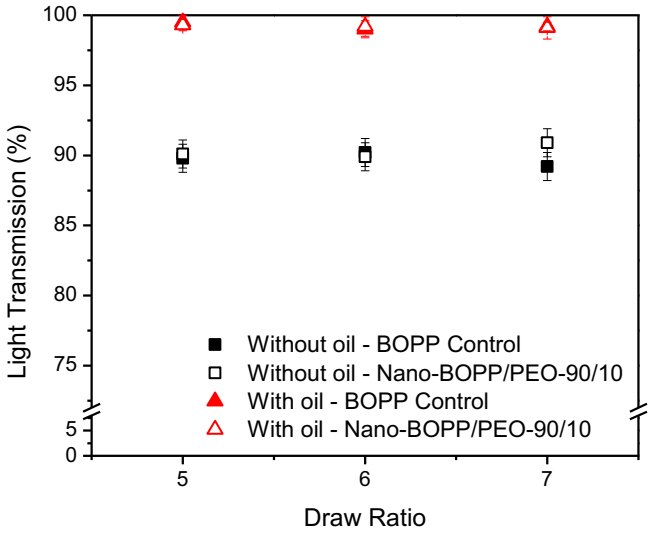

Fig. 8. Light transmission results of BOPP control films and nano-BOPP films that were stretched at 145 °C.

Two other key properties of the polymer film are transparency and toughness. Additional experiments revealed that the nano-BOPP had the same excellent transparency as control films, Fig. 8. With the use of a refractive index matching oil to remove the effect of surface roughness, the light transmission was almost 100%. Up to 10 vol.% PEO was incorporated without any detrimental effect on the clarity due to the nanometer thickness of the PEO crystals, which was well below the quarter wavelength of visible light.

The PEO single crystals in nano-BOPP film actually increased the tear energy by about 10% compared to control film without the PEO, Fig. 9. In nano-BOPP film, the PEO single crystals served as crack deflectors and increased the crack path length [17].

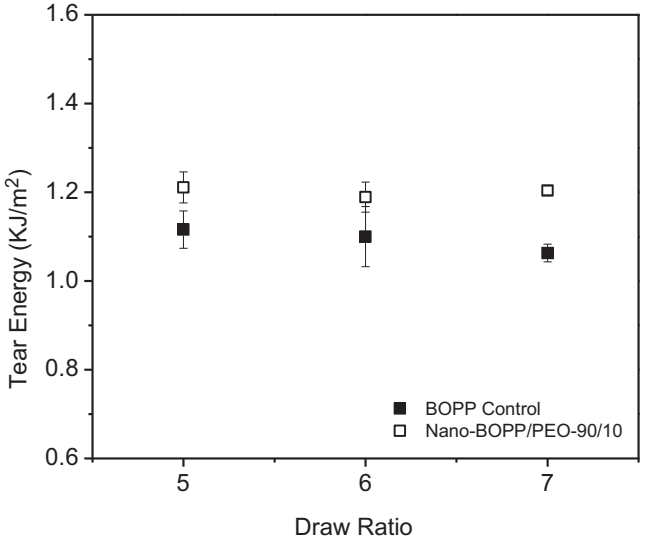

Fig. 9. Effect of PEO nanolayers on the tear energy. Films were stretched at 145 °C to various draw ratios.

4. Conclusions

Here we demonstrated a new concept for achieving nanoscale reinforcement of polyolefin film by combining layer-multiplying coextrusion with biaxial orientation. Coextrusion created a hierarchical layered structure of PP and PEO. Biaxial orientation exploited stretching and subsequent confined crystallization to transform spherulitic PEO microlayers *in situ* into impermeable nanolayers of highly oriented lamellar single crystals. Formation of highly oriented PEO lamellae was due to the confinement under which the melted PEO nanolayers recrystallized, and was not due to the biaxial stretching process. In contrast, biaxial stretching transformed the PP layers into an oriented, transparent fibrillar network characteristic of the BOPP control film. The PEO lamellar single crystals improved the oxygen barrier by an order of magnitude without sacrificing clarity and tear resistance. On the other hand, performance of the PEO barrier layers was limited to some extent by the water sensitivity of PEO, and by the relatively low melting temperature of the PEO lamellae. Future research needs to identify other polymers that crystallize as high barrier nanolayers and are less water-sensitive with higher melting temperature. Nevertheless, the study demonstrates how packaging strategies can be designed and executed to achieve the right barrier properties. Layer-multiplying coextrusion, which is readily adapted to existing commercial processes, now makes it possible to incorporate nano-reinforcement into conventional polyolefin films.

Acknowledgements

This research was supported by the *NSF Center for Layered Polymeric Systems* (Grant DMR-0423914).

References

[1] Podsiadlo P, Kaushik AK, Arruda EM, Waas AM, Shim BS, Xu J, et al. Science 2007;318:80–3.
[2] Bharadwaj RK. Macromolecules 2001;34:9189–92.
[3] Usuki A, Kojima Y, Kawasumi M, Okada A, Fukushima Y, Kurauchi T, et al. J Mater Res 1993;8:1179–84.
[4] Kojima Y, Usuki A, Kawasumi M, Okada A, Fukushima Y, Kurauchi T, et al. J Mater Res 1993;8:1185–9.
[5] Ray SS, Okamoto MP. Prog Polym Sci 2003;28:1539–641.
[6] Paul DR, Robeson LM. Polymer 2008;49:3187–204.
[7] Wang HP, Keum JK, Hiltner A, Baer E, Freeman B, Rozanski A, et al. Science 2009;323:757–60.
[8] Wang HP, Keum JK, Hiltner A, Baer E. Macromolecules 2009;42:7055–66.
[9] Tanaka H, Masuko T, Okajima S. J Polym Sci Part A-1 Polym Chem 1969;7:3351–61.
[10] Campbell C, Viras K, Richardson MJ, Masters AJ, Booth C. Makromol Chem 1993;194:799–816.
[11] Lin YJ, Dias P, Chum S, Hiltner A, Baer E. Polym Eng Sci 2007;47:1658–65.
[12] Baer E, Hiltner A, Keith HD. Science 1987;235:1015–22.
[13] Dias P, Lin YJ, Hiltner A, Baer E, Chen HY, Chum SP. J Appl Polym Sci 2008;107:1730–6.
[14] Lin YJ, Dias P, Chen HY, Hiltner A, Baer E. Polymer 2008;49:2578–86.
[15] Cussler EL, Hughes SE, Ward WJ, Aris R. J Membr Sci 1998;38:161–74.
[16] Tadokoro H, Chatani Y, Yoshihara T, Tahara S, Murahashi S. Makromol Chem 1964;73:109–27.
[17] Gent AN, Jeong J. J Mater Sci 1986;21:355–63.